Available online at www.sciencedirect.com

ScienceDirect

Procedia Computer Science 70 (2015) 304 – 310

Procedia Computer Science

4th International Conference on Eco-friendly Computing and Communication Systems (ICECCS)

Remote sensing image fusion using PCNN model parameter estimation by Gamma distribution in shearlet domain

Biswajit Biswas[a,*], Biplab Kanti Sen[a], Ritamshirsa Choudhuri[a]

[a] *University of Calcutta, 92-A.P.C road, Kolkata and 700009, India*

Abstract

Here the proposed approach deals with some adaptive parameters in pulse coupled neural network (PCNN) model which are highly suitable in image fusion. Initially, the source images are separately decomposed into multi-scaled and multi-directional bands by shearlet transform (ST). Later, the PCNN model is mapped between the decomposed low pass ST sub-bands which depends on linking pulse response and coupling strength with regional statistics of ST coefficients. The process of different high pass ST sub-bands and utilization of singular value decomposition (SDV) have been discussed in details. Finally, we have obtained fusion results by the inverse shearlet transformation (IST). The experimental results on satellite images show that the proposed method has good performance and able to preserve spectral information and high spatial details simultaneously like the original source images. The objective evaluation criteria and visual effect illustrate that our proposed method has a better edge over the prevalent image fusion methods.

Peer-review under responsibility of the Organizing Committee of ICECCS 2015

Keywords: Remote sensing image fusion, shearlet transform, pulse code neural network, single value decomposition, gamma distribution, spectral angle mapper

1. Introduction

Mainly remote sensing images are obtained from multiple satellite image sensors [1]. Now satellite imaging system produces high spatial PAN and multi-spectral MS images which are widely utilized in the arenas of remote sensing image analysis, feature extraction, modeling, image classification, target detection and recognition [1,3]. Generally, image fusion can be defined as the combination of visual information contained in any number of source images into a single fused image without any kind of spectral distortion or information loss [3,4]. In practice, the most image fusion method are performed at the pixel level. Most pixel-level image fusion schemes are Intensity-Hue-Saturation (IHS) technique [1], Principal Components Analysis (PCA) approach [1], Bravery Transform (BT) [1], Gram-Schmidt technique (GST) [2], Laplacian pyramid method (LP) [1], Gaussian contrast pyramid [2] and different statistical based schemes such as *MS+PAN sharpening* [2], Bayesian approach [3], Markov Random Fields approach [3] as well as various soft computing

* *E-mail address:* biswajit.cu.08@gmail.com

Peer-review under responsibility of the Organizing Committee of ICECCS 2015
doi:10.1016/j.procs.2015.10.098

approach[1,3] etc. Based on multi-resolution theory, different pixel-level wavelet-based image fusion techniques like discrete wavelet transform (DWT)[1,6], complex wavelet transform (CxWT)[6,9], *â trous* wavelet transform (TDWT)[1,9] and etc. have been developed which produces high quality fused images. As known , images fused by wavelets suffer from lack of spatial information, salient features and loss of geometrical information[6,9]. Also Multi-scale geometric analysis (MGA) is an efficient computational and special version of MSD model which can analysis the multi-resolution and geometric nature of a high dimensional signal[6,9]. Various MGA models have successfully been developed like ridgelet, curvelet, contourlet, bandlet, shearlet which are discussed in[6,9]. These MGA methodologies are highly effective to represent edge information than wavelet systems and are appropriate for extracting geometrical information from an image[6,9]. Shearlets is a new MGA methodology that equipped with a tight Parseval frame at various scales and directions, and optimally sparse in representing the geometric quality of an image such as edges[9].

In this work, we have applied the benefits of ST and PCNN to implement a new fusion framework which can process and combine ST coefficients adeptly. PCNN have been effectively utilized in the proposed fusion scheme. The advantages of SVD have efficiently been utilized in this method to normalize the PAN image as compatible with MS image to avoid the spectral deformation. The low pass ST sub-bands are processed and the largest low pass ST sub-bands are fused by PCNN. The approach evaluates the related high pass ST sub-bands and the directional ST sub-bands of the images at different decomposition levels. Finally reconstruction of the fused image by inverse ST has been performed. Experimental results demonstrate the efficiency of the proposed fusion technique for analysis of remote sensing satellite images.

The rest of this paper is organized as follows. A brief introduction of ST is given in Section 2. Section 3 introduces PCNN. Techniques for construction and modification of low pass and high pass ST bands are illustrated given in Section 5. The fused results and discussions are briefed in Section 6. Finally, we conclude this paper in section 7.

2. Shearlet transform

Typically, ST have been developed based on an affine system with composite dilations[9,10]. Let us briefly discuss the continuous and discrete ST at the fixed resolution level j in the following subsections.

2.1. Continuous shearlet system

In dimension $n = 2$, the affine systems with composite dilations are the collections represented as[9,10]:

$$\Psi_{AB}(\psi) = \{\psi_{j,k,l}(X) = |\det A|^{j/2}\psi\left(B^l A^j X - k\right) : j,l \in \mathbb{Z}, k \in \mathbb{Z}^2\} \tag{1}$$

where, A, B are 2×2 invertible matrices, $f \in L^2(\mathbb{R}^2)$, mostly represented as follows:

$$\sum_{j,k,l} |\langle f, \psi_{j,k,l}\rangle|^2 = ||f||^2 \tag{2}$$

The elements of this system are known as composite wavelets if $\Psi_{AB}(\psi)$ forms a Parseval frame or tight frame for $f \in L^2(\mathbb{R}^2)$. In this system, the dilations matrices A^j are the scale transformations, while the matrices B^l are the area-preserving geometric transformations, such as rotations and shear.

As stated in the continuous ST, we have[9],

$$\psi_{a,s,k}(x) = a^{-3/4}\psi\left(U_s^{-1}V_a^{-1}(x-k)\right) \tag{3}$$

where $V_a = \begin{pmatrix} a & 0 \\ 0 & \sqrt{a} \end{pmatrix}$, $U_s = \begin{pmatrix} 1 & 0 \\ 0 & 1 \end{pmatrix}$, $\psi \in L^2\left(\mathbb{R}^2\right)$, also satisfy the following conditions[9]:

1. $\hat{\psi}(\varepsilon) = \hat{\psi}(\varepsilon_1, \varepsilon_2) = \hat{\psi}_1(\varepsilon_1)\hat{\psi}_2(\varepsilon_2/\varepsilon_1)$;
2. $\hat{\psi}_1 \in \mathscr{C}^\infty(\mathbb{R})$ $\text{supp}\psi_1 \subset [-2,-1/2] \bigcup [1/2,2]$, where, ψ_1 is continuous wavelet;
3. $\hat{\psi}_2 \in \mathscr{C}^\infty(\mathbb{R})$ $\text{supp}\psi_2 \subset [-1,1], \hat{\psi}_2 > 0$ But $\|\psi_2\| = 1$

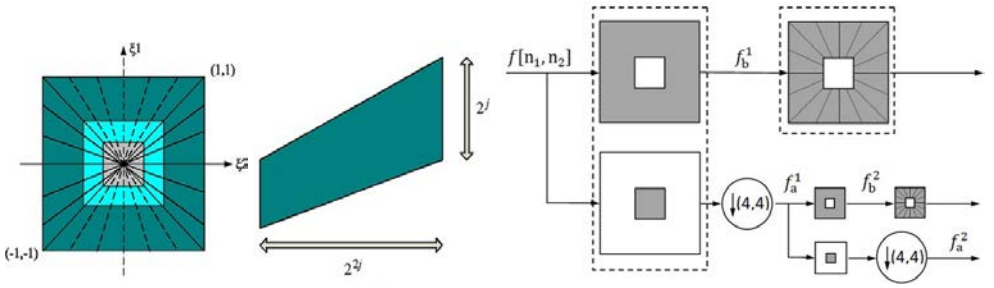

Fig. 1: The structure of the frequency tiling by the ST: (a) The tiling of the frequency plane $\mathbb{R}^2$ induced by the ST, (b) The size of the frequency support of a ST $\psi_{j,l,k}$, (c) The multi-scale and multi-directional decompositions of ST[9].

For $\psi_{a,s,k}, a \in \mathbb{R}^+$, $s \in \mathbb{R}^+$ and $k \in \mathbb{R}^+$, for any $f \in L^2(\mathbb{R}^2)$, is called shearlet, more specifically a collection of wavelets with different scales. Here, the anisotropic expansion matrix U_s is associated with the scale transform and the shear matrix V_a specify the geometric transformation. Mostly, $a = 4$ and $s = 1$. Where a, s, k are specified as scale transformations, shear direction and translation vector respectively.

2.2. The discrete shearlet system

The process of the discrete ST can be divided into two steps such as multi-scale subdivision and direction localization[9,10]. Figure1 shows an example decomposition process using ST.

In this system, at any scale j, let $f \in L(\mathbb{Z}_N^2)$. Firstly, the Laplacian pyramid method is used to decompose an image f_a^{j-1} into low pass image f_a^j and a high pass image f_h^j with $N_j = N_{j-1}/4$, where $f_a^{j-1} \in L(\mathbb{Z}_{N_{j-1}}^2)$, $f_a^j \in L(\mathbb{Z}_{N_j}^2)$ and $f_h^j \in L(\mathbb{Z}_{N_{j-1}}^2)$. After decomposition, we estimate $\hat{f}_b^j$ on a pseudo-polar grid with the one-dimensional band pass filter based on the signal components, which generate a matrix $D\hat{f}_b^j$. Then, we apply a band-pass filter on matrix $D\hat{f}_b^j$ to reconstruct the Cartesian sampled values straightforwardly and also apply the inverse two-dimensional Fast Fourier Transform (FFT) to reconstruct the image[9].

3. PCNN model

The components of the simple PCNN neurons form the receptive field, modulation domain and pulse generating domain[7,8]. The receptive field are given as follows[7,8]:

$$F_{ij}[n] = S_{ij}[n]; L_{ij}[n] = e^{-\alpha_L} L_{ij}[n-1] + V_T \sum_{kl} W_{ijkl} Y_{kl}[n-1] \tag{4}$$

Modulation domain is given as follow:

$$U_{ij}[n] = F_{ij}[n]\,(1 + \beta L_{ij}) \tag{5}$$

and Pulse generating domain are given as follows:

$$Y_{ij}[n] = \begin{cases} 1 & \text{if } U_{ij}[n] > T_{ij}[n] \\ 0 & \text{otherwise} \end{cases}, T_{ij}[n] = e^{-\alpha_T} T_{ij}[n-1] + V_T Y_{ij}[n] \tag{6}$$

where F_{ij} is exterior outputs. S_{ij}, $S_{ij}[n]$ are denote the input stimulus, n denotes the iterative steps and L_{ij} represents the linking input. The parameter β denotes the connecting weight. w_{ijlk} denotes the synaptic links. V_L, V_T represents the magnitude scaling term of threshold potential as a normalization constant. P_{ij} denotes the output pulse of a neuron whose value is either 0 or 1. T_{ij} is the dynamic threshold. α_T is a constant. U_{ij} represents the firing map of the image which is related with the inner activity of the neuron. The fused images is obtained by using U_{ij}. If $U_{ij}[n] > T_{ij}[n]$[7,8].

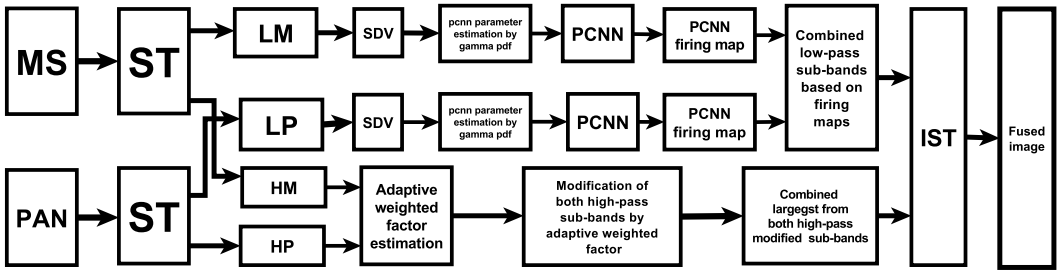

Fig. 2: Schematic diagram of PCNNST-based fusion algorithm.

4. Singular value decomposition (SVD)

Singular value decomposition (*SVD*) is a technique which orthogonally decomposes a given matrix into a singular value matrix which contains only a few non-zero values. Usually, *SVD* of an $\mathbf{m} \times \mathbf{n}$ matrix $\mathbf{A}$ is given by[5]:

$$\mathbf{A} = \mathbf{U_X} \Sigma_A \mathbf{V_A^T} \tag{7}$$

where the columns of the $\mathbf{m} \times \mathbf{n}$ matrix, $\mathbf{U_A}$ are known as *left singular vectors*, the rows of the $\mathbf{n} \times \mathbf{n}$ matrix $\mathbf{V_A^T}$ contain the elements of the *right singular vectors*, and the diagonal elements of the $\mathbf{n} \times \mathbf{n}$ diagonal matrix $\Sigma_A = \mathsf{diag}(\sigma_1, \sigma_2, \cdots, \sigma_n)$ are known as the *singular values*[5]. Moreover, $\sigma_i > 0$ for $0 \leq i \leq q$ and $\sigma_i = 0$ if $(q+1) \leq i \leq n$. In notational convenience, $(\sigma_1 \geq \sigma_2 \geq \cdots \geq \sigma_q \geq 0)$[5].

5. Fusion schemes for shearlet coefficient

In this work, we have named the proposed fusion scheme as *Pulse Code Neural Network in Shearlet Transform (PCNNST)*. The main steps of the PCNNST scheme are schematically demonstrated in Fig. 2. The role of all implemented processes are discussed as follows:

5.1. Application methodology of PCNN in fusion of low pass sub-bands

In this study, L_{PAN} the high spatial ST PAN image which contains higher coefficient values than L_{MS} image. In order to normalize the coefficient values of L_{PAN} which be compatible with the coefficient values of L_{MS}, the L_{PAN} and L_{MS} are modified by SVD. Applied SVD on both L_{PAN} and L_{MS} separately and determined a ratio parameter. The parameter is modified each singular value of L_{PAN} and L_{MS}. Normalization of ST coefficients of L_{PAN} and L_{MS} are performed as follows:

$$[U_{MS}, \Sigma_{MS}, V_{MS}] = SVD_{MS}(L_{MS}), [U_{PAN}, \Sigma_{PAN}, V_{PAN}] = SVD_{PAN}(L_{PAN}) \tag{8}$$

where $\Sigma_{MS}, \Sigma_{PAN}$ are singular values of L_{MS} and L_{PAN} respectively. To generate a normalized $\hat{L}_{PAN}$ matrix from L_{PAN} image, an adaptive factor, ϕ is computed by forming a ratio with Σ_{MS} and Σ_{PAN} and dividing it by a weighted factor W. This is represented as follows:

$$\phi = \frac{\sum_s \max(\Sigma_s)}{w * \sum_s (\Sigma_s)} \tag{9}$$

where $w = \sqrt{(\log(r * c))}$, r and c are row and columns of L_{PAN}. Finally, we regenerate the normalized L_{PAN} by using inverse SVD technique as shown below:

$$\hat{L}_{PAN} = V_{PAN} * \left(\frac{\phi}{2} * \Sigma_{PAN}\right) * U_{PAN}^T, \hat{L}_{MS} = V_{MS} * ((2 * \phi *)\Sigma_{MS}) * U_{MS}^T \tag{10}$$

where $\hat{L}_{PAN}$ and $\hat{L}_{MS}$ are the normalized image. In order to combined of both normalized $\hat{L}_{MS}$ and $\hat{L}_{PAN}$, PCNN is processed. In PCNN, receptive field, modulation domain and pulse generating domain for both L_{MS} and L_{PAN} as follows:

The receptive field:

$$F_{ij}^{MS}[n] = S_{ij}^{MS}[n], F_{ij}^{PAN}[n] = S_{ij}^{PAN}[n], L_{ij}[n] = e^{-\alpha_L} L_{ij}[n-1] + V_T \sum_{kl} W_{ijkl} Y_{kl}[n-1] \tag{11}$$

Modulation domain:

$$U_{ij}[n] = \max\left(F_{ij}^{MS}[n]\left(1+\beta_{ij}^{MS}L_{ij}\right), F_{ij}^{PAN}[n]\left(1+\beta_{ij}^{PAN}L_{ij}\right)\right) \tag{12}$$

Pulse generating domain:

$$Y_{ij}[n] = \begin{cases} 1 & \text{if } U_{ij}[n] > T_{ij}[n] \\ 0 & \text{otherwise} \end{cases}, T_{ij}[n] = e^{-\alpha_T} T_{ij}[n-1] + V_T Y_{ij}[n] \tag{13}$$

where $\beta_{ij}^{MS}, \beta_{ij}^{PAN}$ of PCNN model are evaluated by regional statistics of L_{MS} and $\hat{L}_{PAN}$. In this study, these parameters are estimated by using maximum likelihood estimation of generalized gamma distribution[10]. The parameter α is estimated by applying Kullback-Leibler distance (KLD) metric[10]. In mathematical convenience, the generalized gamma distribution $X \sim GGD(\alpha, \beta)$ with pdf

$$p(x;\alpha,\beta) = \frac{\beta}{2\alpha\Gamma(1/\beta)} \exp^{-\left(\frac{|x|}{\alpha}\right)^{\beta}} \tag{14}$$

where $\Gamma(\cdot)$ is the Gamma function . The KLD between two PDFs is defined as :

$$KLD(p(x;\theta_s) \| p(x;\theta_t)) = \int (p(x;\theta_s) \log \frac{p(x;\theta_s)}{p(x;\theta_t)} \partial x \tag{15}$$

The parameters of the proposed method were: Initialize internal activity $U_{ij} = 0$, linking input $L_{ij} = 0$, threshold $T_{ij} = 0$. The maximum iterative time was 200 and the linking arrange parameter was 3. Magnitude scaling term of threshold potential $V_T = \hat{\alpha} * \hat{\beta}$, $\beta_{ij}^{MS} = \alpha_{\hat{MS}}/w$, $\beta_{ij}^{PAN} = \alpha_{\hat{PAN}}/w$ and $W_{ij} = \frac{1}{\sqrt{((i-LA_x).^2+(j-LA_y).^2)}}$, where LA is a weighted matrix defined by linking arrange parameter.

5.2. Fusion rule for high frequency shearlet coefficient

In PCNNST, a new decision map have been developed to improve the high pass ST sub-bands and an efficient fusion rule which combines improved high pass ST sub-bands automatically. Let $H_\iota^{l,k}(x,y)$ be the high pass ST coefficient at the location (x,y) in the l^{th} sub-band at the k^{th} level and $\iota = PAN, MS$. For the current ST sub-band $H_\iota^{l,k}$, let $Q_{\iota,h}$ be the sum of $H_\iota^{l,k}$ and other horizontal ST sub-bands $H_\iota^{m,k}$ for the level k. It can be estimated by:

$$Q_{\iota,h} = \sum_{k=1}^{K} \sum_{l=1}^{L} \|(H_\iota^{l-1,k}, H_\iota^{l,k})\| \tag{16}$$

where $\|\cdot\|$ is the Manhattan distance. Likewise, let $Q_{\iota,v}$ be the sum of $H_\iota^{l,k}$ and all other vertical high pass ST sub-bands $H_\iota^{m,n}$ for the different finer levels. It can be evaluated by:

$$Q_{\iota,v} = \sum_{l,m=1}^{K} \sum_{k,n=1}^{L} \|(H_\iota^{l,k}, H_\iota^{m,n})\| \tag{17}$$

To determine the parameter $\tau_{\iota,h}$ along horizontal and the parameter $\tau_{\iota,v}$ along vertical high pass ST sub-bands for the present high pass ST sub-band $H_\iota^{l,k}$, we perform:

$$\tau_{\iota,h} = \sqrt{\frac{Q_{\iota,h}}{(Q_{\iota,h}+Q_{\iota,v})}}, \tau_{\iota,v} = \sqrt{\frac{Q_{\iota,v}}{(Q_{\iota,h}+Q_{\iota,v})}} \tag{18}$$

Table 1: Quantitative comparison and result analysis in Fig. 3

Method	AWLP	GIHS	PST	PCNNST
RASE	20.5847	21.6973	17.7164	**11.8230**
ERGAS	1.5376	1.1942	1.3149	**0.8961**
SAM	0.758	0.876	0.618	**0.627**
$Q4$	0.9574	0.9589	0.9697	**0.9841**
$Q^{F/AB}$	0.7528	0.6594	0.6971	**0.8706**

The parameter $\tau_{l,h}$ is a relationship between $H_l^{l,k}$ and other neighboring high pass ST sub-bands in the same horizontal plane and $\tau_{l,v}$ is a relationship between $H_l^{l,k}$ for the different vertical planes with its corresponding neighboring ST sub-bands. Then, estimation of the new coefficients $H_{l,new}^{l,k}$ using parameters $\tau_{l,h}$ and $\tau_{l,v}$, is given by:

$$H_{l,new}^{l,k} = H_l^{l,k} \times \sqrt{1+\tau_{l,h}^2+\tau_{l,v}^2} \tag{19}$$

Finally, the fused high pass ST sub-band coefficients $H_F^{l,k}(x,y)$ is obtained by the following estimation:

$$H_F(x,y) = \left\{ H_{PAN,new}^{l,k}(x,y), \text{if} H_{PAN,new}^{l,k} \geq H_{MS,new}^{l,k}; H_{MS,new}^{l,k}(x,y) \text{otherwise} \right. \tag{20}$$

6. Analysis of experimental results

Experimental simulation platform is *MATLAB R2012b in the PC with the Intel (R) core (TM) 2 Quad CPU 2.4 GHz and 16 GB RAM*. A variety of quality metrics are used for the assessment of the fusion performance quantitatively such as relative average spectral error (RASE)[11,12], ERGAS[2,11], spectral angle mapper (SAM)[4,11], $Q4$ index[11,12], and $Q^{AB/F}$[12]. To evaluate the performance of PCNNST fusion of PAN and MS image, a valid experiment is implemented and the results are compared with four different typical fusion schemes : (1) *Average Weighted Laplacian pyramid method (AWLP)*[1], (2) *Generalized Intensity-Hue-Saturation(GIHS) method*[2], (4) *MS+PAN Sharpening Technique (PST)*[1,4], respectively. To fuse PAN image with size 512×512 and MS image with size 512×512 the running time of the proposed technique have take average $5.975m$[13]. The AWLP, and GIHS methods need less than $76.215s$. The execution time of the PST method is about $1.535m$. Compared with the above mentioned methods, the proposed method is more time consuming but rate of the algorithm can be significantly increased with graphics processing unit (GPU).

The performance results estimated by using RASE, ERGAS, SAM, $Q4$ index and $Q^{AB/F}$ are shown in Table 1 of PCNNST and different fusion methods separately. The highest score in each row of Tables 1is demonstrated in bold. From the table 1, it can be noted that the PCNNST method consistently outperforms the other methods in both evaluation metrics. In addition to objective evaluation, we have also performed a visual comparison on images as shown in Fig. 3. The resulting fused images obtained from the AWLP, GIHS, PST and PCNNST respectively are shown in Fig. 3. Experiments show that PCNNST approach can resolve spectral distortion problems and successfully preserve the spatial information of a PAN image. The results of RASE and ERGAS demonstrate that the proposed method produces the best value in comparison to others. As to the SAM and $Q^{AB/F}$ index, the AWLP, PST methods are provide good results, whereas GIHS suffers from spectral distortion. The PST method is offer improved quality of fusion. The proposed method PCNNST provides enhanced multi-spectral fused image with high spatial resolution and color information. Superiority of our method is demonstrated by comparing best SAM, RASE, ERGAS, $Q4$ and $Q^{AB/F}$ index results.

7. Conclusion

In this paper, we present a new remote sensing satellite image fusion technique based on ST and PCNN. In our methodology, we first decompose the source image using ST and then apply the PCNN technique on those decomposed levels. We then select the best ST coefficients to preserve the spectral information. For the high frequency

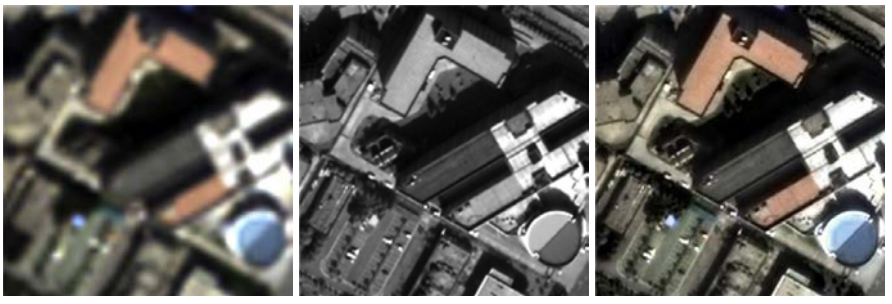

(a) *MS* (b) *PAN* (c) *AWLP*

(d) *GIHS* (e) *PST* (f) *PCNNST*

Fig. 3: QuickBird MS, PAN image [13], and the resulting images using different fusing methods. (a) MS; (b) PAN; (c) AWLP; (d) GIHS; (e) PST; (f) PCNNST.

sub-band coefficients, a novel process is presented. The objective is to preserve the geometrical details and spectral information of the source images. All comparisons made demonstrate that the proposed method outperforms conventional fusion techniques in terms of both visual quality and quantitative evaluation criterion.

References

1. Wang Z, Ziou D, Armenakis C, Li D, and Li Q. A Comparative Analysis of Image Fusion Methods. IEEE TRANSACTIONS ON GEOSCIENCE AND REMOTE SENSING 2005;43(6), p.1391-1402.
2. Zhou X, Liu J, Liu S, Cao L, Zhou Q. and Huang H., A GIHS-based spectral preservation fusion method for remote sensing images using edge restored spectral modulation, ISPRS(JPRS) 2014; 88, p.16-27.
3. Chen S, Guo Q, Leung H, and Bosse E. A Maximum Likelihood Approach to Joint Image Registration and Fusion, IEEE TRANSACTIONS ON IMAGE PROCESSING 2011; 20(5), p.363-1372.
4. Xu M, Chen H, and Varshney PK. An Image Fusion Approach Based on Markov Random Fields, IEEE TRANSACTIONS ON GEOSCIENCE AND REMOTE SENSING 2011; 49(12), p.5116-5127.
5. Nasir H, Stankovic V, and Marshall S. Singular value decomposition based fusion for super-resolution image reconstruction, Signal Processing: Image Communication 2011.
6. Do MN and Vetterli M. The contourlet transform: An efficient directional multiresolution image representation, IEEE Trans. Image Proc 2005; 14(12), p.2091-2106.
7. Kong W, Zhang L, and Lei Y. Novel fusion method for visible light and infrared images based on NSST-SF-PCNN, Infrared Physics & Technology 2014; 65, p.103-112.
8. Xiang T, Yan L, and Gao R. A fusion algorithm for infrared and visible images based on adaptive dual-channel unit-linking PCNN in NSCT domain, Infrared Physics & Technology 2015; 69, p.53-6
9. Easley G, Labate D, Lim WQ. Sparse directional image representations using the discrete ST, Appl. Comput. Harmon. Anal 2008; 25, p.25-46.
10. Wang L, Li B, Tian L. EGGDD: An explicit dependency model for multi-modal medical image fusion in shift-invariant ST domain, Information Fusion 2013.
11. Zhang Y. Methods for image fusion quality assessment-A review, comparison and analysis, Int. Arch. Photogramm. Remote Sens. Spatial Inf. Sci 2008; XXXVII(B7), p.1101-1109.
12. Xydeas CS, Petrovic V. Objective image fusion performance measure, Electron; Lett 2000. 36, p. 308-309.
13. http://glcf.umiacs.umd.edu.